Full Length Research Paper

Modeling of rapeseed at maturity stage using 3D unorganized point clouds and digital images

Ruifang ZHAI [1], Xiu JING[1]*, Chengda LIN[2], Hui PENG[1] and Jun LUO[1]

[1]Research Institute for Computer Applications, Huazhong Agricultural University, Wuhan, 430070, P. R. China.
[2]College of Resource and Environment, Huazhong Agricultural University, Wuhan, 430070, P. R. China.

Creating 3D plant models is often a difficult and laborious task. To make it easier and more natural, the integration of digital images and 3D unorganized point clouds from a digitizer provides a promising approach for rapeseed model generation. In the present study, 3D unorganized point clouds and digital images were incorporated in the generation of complex models of rapeseeds at maturity stage. Unorganized point clouds and image sequences were taken from different viewpoints using a 3D digitizer. The 3D unorganized points and image sequences were used for the automated registration of all data sets from all the viewpoints, which is pair-wise registration. Later, all the pair-wise registration parameters were used as initial transformation parameters for multiple registrations. The next procedure generated a surface model by triangulated irregular network using all the point clouds. The capabilities of our system were demonstrated through real data sets. Experimental results showed that the average normal distances between the two scans were less than 0.3 mm after simultaneous registration, which indicated that the proposed methodology is effective and efficient.

Key words: Rapeseed, 3D modeling, unorganized point clouds.

INTRODUCTION

Rapeseed is a crop grown mainly for its high-quality oil and protein. It provides a versatile kind of oil, which is used for cooking and frying as well as fuel or raw material for the chemical industry. In the face of global climate change, rapeseed can play an important role as a future source of renewable energy. The morphogenesis and architecture of rapeseed at maturity stage are critical factors affecting the estimation of seed yields. However, they are not yet fully studied because of the structure complexity of the rapeseed at maturity stage as well as the lack of appropriate tools for three-dimensional (3D) measurements. Studies on rapeseed have mainly

focused on its color detection, nutrition information extraction of rape canopy, leaf information studies, and plant modeling (Guan, 2007; Yuan et al., 2009; Zhang et al., 2006).

Recently, several methods have been developed to measure the 3D structure of entire objects in a non-destructive manner, including the use of a 3D digitizer, digital stereo photogrammetry, X-ray computed tomography, or phase-shifting projected fringe profilometry with some adaptation toward the quantification and visualization of 3D plant structures (Dornbushch, 2007). Among these methodologies, the 3D digitizer, also known
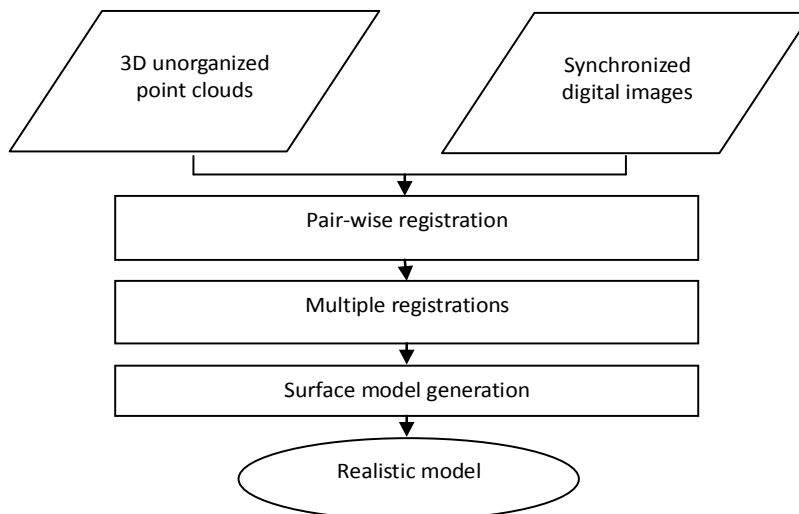
Figure 1. Flowchart of the proposed methodology.

as the 3D scanner, is a new device that can retrieve 3D data of a solid object by simply projecting light on to it. Compared with other methods, the advantage of using a digitizer is that it does not come into contact with the object, thus avoiding damage to the object being studied. Studies on the use of the 3D digitizer have mainly focused on maize (Ma et al., 2006), tomato (Masaaki and Yosuke, 2005), rice (Watanabe et al., 2005), and other plant models (Dornbushch et al., 2007).

However, measuring rapeseed using the 3D digitizer has rarely been reported. In the present study, the main objective is to evaluate the performance of using the 3D digitizer to generate the complex rapeseed model at maturity stage. The flowchart of the process is shown in Figure 1.

The process starts by taking 3D digitizer generated unorganized point clouds and image sequences from different viewpoints. Next, the unorganized points and the image sequence are used for the registration of all the data sets from all viewpoints, thus resulting in a complete rapeseed model. The registration approach includes pair-wise and multiple surface registration procedures that have been developed to combine all the scans into a common reference frame. The next procedure generates a surface model through a triangulated irregular network (TIN) using all the point clouds. Finally, the capabilities of the proposed system are demonstrated through real data sets. Quantitative and qualitative assessments of the results are also discussed.

MATERIALS AND METHODS

Experimental system and data acquisition

The experimental equipment consisted of a 3D digitizer (VIVID 910)

Figure 2. The hardware system.

from Konica Minolta, a rotatable platform on which the rapeseed was placed, a mechanical impulse device, a personal computer, and data acquisition software called polygon editing tool. The VIVID 910 digitizer (Figure 2) uses laser-beam light sectioning technology to scan work pieces using a slit beam. Light reflected from the work piece is acquired using a charge-coupled device (CCD) camera. Afterwards, the 3D data were created by triangulation in order to determine distance information. The laser beam was scanned using a high-precision galvanometric mirror; 640×480 individual points were measured per scan. In addition to distance data, this 3D digitizer was also used to acquire color image data. Using a rotating filter to separate the acquired light, the VIVID 910 digitizer created color image data for 640×480 points with the same CCD as that used for distance data. The software was used mainly to control the experimental setup and analyze the results.

The rotatable platform was designed to capture data sets in a convenient way. It consisted of a planar patch, which was a stepper
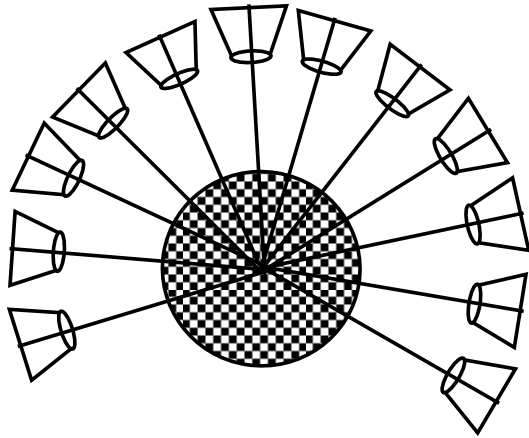
(a)

(b)

(c)

Figure 4. (a) The acquired digital images at certain viewpoints; (b) The corresponding 3D point clouds; (c) The coordinates of the 3D unorganized point clouds.

Figure 3. The methodology of data acquisition.

motor that can drive the platform to rotate. The object was placed on the center of the rotatable platform. Once the platform was driven to rotate at a given angle (that is, 12°), the digitizer captured the data sets one at a time. In this way, the sequential data sets of the object were acquired automatically (Figure 3). The data sets included 3D unorganized point clouds and their corresponding digital images. Some of these recorded from specific viewpoints are shown in Figure 4. The data sets from one viewpoint included one scan (3D unorganized point clouds) and one digital image, as shown in Figure 4a and b, respectively. Figure 4c presents the 3D coordinate values of the unorganized point clouds from one viewpoint, which would be used for later procedures.

Experimental Procedure

With the rotation of the rotatable platform at a given angle, one scan (represented by unorganized point clouds) and its corresponding digital image were taken at that viewpoint until the turntable finished one complete circle. Given that one scan was unable to represent the whole structure of the object, all the point clouds from different viewpoints were registered into one common reference frame. This process included two procedures, namely, pair-wise and seamless registration of multiple scans. To present the 3D architecture of the objects, we used the unorganized point clouds as well as the interrelations among all these unorganized points. Therefore, the next procedure involved building a surface model through the generated 3D point clouds of the entire rapeseed. Finally, a realistic 3D model of rapeseed at maturity stage was obtained, and its accuracy was also estimated.
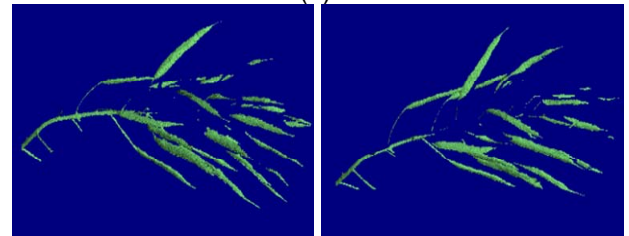
Pair-wise registration

The registration of two scans played an important role in the rapeseed model generation. However, considering the complexity of the plants and the characteristics of unorganized point clouds, it is difficult to find two conjugate points among the unorganized point clouds from two adjoining viewpoints. According to the correspondent relations between one scan and the digital image at the same viewpoint, the model provided a promising way to find conjugate points for registration between the two scans at different viewpoints.

By finding conjugate points in the two adjoining digital images, we can locate conjugate 3D points between one adjoining scan pairs. Figure 5 shows the matched conjugate points from two adjoining digital images. According to the inner corresponding relations between digital image and the scan from one viewpoint, the conjugate 3D points were located between the two scans. Using more than three conjugate points in two 3D scans, the transformation parameters between individual pairs were computed effectively given by:

$$\begin{bmatrix} X'_p \\ Y'_p \\ Z'_p \end{bmatrix} = \begin{bmatrix} X_T \\ Y_T \\ Z_T \end{bmatrix} + SR(\Phi, \Omega, K) \begin{bmatrix} X_p \\ Y_p \\ Z_p \end{bmatrix} \qquad (1)$$

Where: X_p, Y_p, Z_p are the coordinates of a point from Scan 1;

X_T, Y_T, Z_T are three translations between the two reference frames;

frames; S is a scale factor between the two reference frames;

Figure 5. Match results of digital images. Red points represent the matched conjugate points from the two digital images.

X_p', Y_p', Z_p' are the coordinates of the transformed point with respect to the reference frame of Scan 2; $R(\Phi, \Omega, K)$ is the rotation matrix between the two reference frames as defined by the rotation angles Φ, Ω, K.

Seamless registration of multiple scans

As mentioned above, n pieces of scans of the rapeseed were obtained, which was essential in developing an effective approach to register all the n scans seamlessly. The n pieces were integrated using the transformation parameters acquired from the pair-wise registration. However, the error propagation of these parameters may possibly lead to error accumulation. In order to minimize such errors, we registered all the scans simultaneously in a multiple surface registration procedure.

The transformation parameters between individual pairs of surfaces were computed through pair-wise surface registration, which was introduced earlier. If the coordinate system of one scan was taken as the reference frame, other scans were transformed from their own reference frames into this common reference coordinate system using the transformation parameters between individual pairs. For one scan, two methods can be used to transform it into the common reference frame, namely, direct and indirect (Figure 6). For example, Scan 9 was integrated into the common reference frame, which was defined by Scan 1, using the pair-wise transformation parameters between Scan 9 and 1. This integration was completed by transforming Scan 9 to 8 first, and then transforming it to Scan 7, and so on, until Scan 9 was transformed into the common reference frame of Scan 1. Ideally, the two transformed scans from Scan 9 to 1 using either the direct or indirect way should be identical. However, this was almost impossible to achieve due to error propagation.

In the present study, 30 scans and the corresponding digital image sequence were obtained. The average normal distances between individual pairs of original scans were less than 0.20 mm. As for the last scan, it was transformed into the common reference frame in two ways. The average distance between the two scans was 0.19 mm in the direct way, whereas that in the indirect way was 4.78 mm. This indicated that the effect of the error propagation was almost inevitable. Therefore, a methodology to refine the registration of n scans was developed. Its aim is to process all the scans simultaneously and solve all the transformation parameters

of all individual scan pairs except for the transformation parameters between the first and the last scan with the initial transformation parameters acquired by Section A.

Assuming there were m scans in the research, Scan 1, 2, …, and m. The transformation function between each scan pair (e.g., Scan i and $i + 1$) could be expressed as follows:

$$SF_i = F_i(SF_{i+1})$$
(2)

where SF_i is Scan i, SF_{i+1} is Scan $i + 1$, and F_i is the transformation function between these two scans.

As for point $P \{X_m, Y_m, Z_m\}$ in the last Scan m, it was transformed directly into the reference frame of Scan 1 to obtain the new coordinate values $\{X_m', Y_m', Z_m'\}$; this is expressed in Equation (1). Meanwhile, the point was transformed into the common reference frame in the indirect way as described previously in order to obtain new coordinate values $\{X_m'', Y_m'', Z_m''\}$; this is expressed in Equation (3). Given that $\{X_m', Y_m', Z_m'\}$ and $\{X_m'', Y_m'', Z_m''\}$ both represent the new coordinates in the reference frame of point $\{X_m'', Y_m'', Z_m''\}$ from Scan m, the two coordinates should be identical as shown in Equation (4) below:

$$\begin{bmatrix} X_m' \\ Y_m' \\ Z_m' \end{bmatrix} = \begin{bmatrix} X_{m,T} \\ Y_{m,T} \\ Z_{m,T} \end{bmatrix} + S_m R_m(\Phi_m, \Omega_m, K_m) \begin{bmatrix} X_m \\ Y_m \\ Z_m \end{bmatrix},$$
(3)

Where: Xm, Ym, Zm are the coordinates of point P in Scan m; X_m', Y_m', Z_m' are the coordinates of the transformed point with respect to the common reference frame of Scan 1 in the direct way; $X_{m,T}, Y_{m,T}, Z_{m,T}$ are three translations between one scan pair, Scan m and Scan 1; $R_m(\Phi_m, \Omega_m, K_m)$ is the rotation matrix between the scan pair Scan m and Scan 1 as defined by the
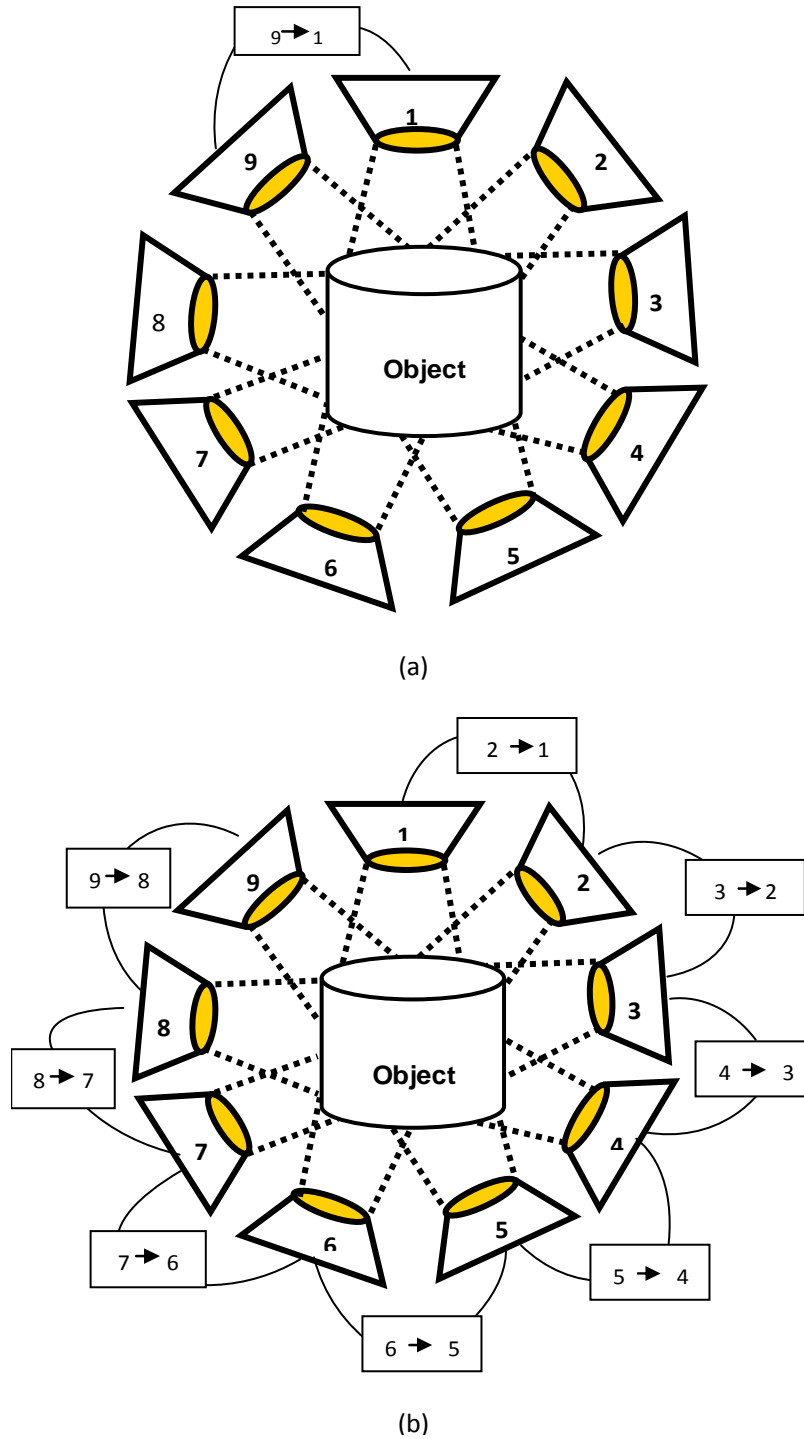
(a)

(b)

Figure 6. Scan 9 could be transformed into the common reference frame (scan 1) either in a direct way (a) or in an indirect way (b).

rotation angles Φ_m, Ω_m, K_m; and S_m is a scale factor between Scan m and Scan 1.

$$\begin{bmatrix} X_m'' \\ Y_m'' \\ Z_m'' \end{bmatrix} = R_1 R_2 \cdots R_{m-1} \begin{bmatrix} X_m \\ Y_m \\ Z_m \end{bmatrix} + \begin{bmatrix} X_{1,T} \\ Y_{1,T} \\ Z_{1,T} \end{bmatrix} + R_1 \begin{bmatrix} X_{2,T} \\ Y_{2,T} \\ Z_{2,T} \end{bmatrix} + R_1 R_2 \begin{bmatrix} X_{3,T} \\ Y_{3,T} \\ Z_{3,T} \end{bmatrix} + \cdots + R_1 R_2 \cdots R_{m-1} \begin{bmatrix} X_{m-1,T} \\ Y_{m-1,T} \\ Z_{m-1,T} \end{bmatrix} \quad (4)$$

In the above equation: X_m, Y_m, Z_m are the coordinates of point P in Scan m; X_m', Y_m', Z_m' are the coordinates of the transformed point with respect to the common reference frame of Scan 1 in the indirect way; $X_{i,T}, Y_{i,T}, Z_{i,T}$ are three translations between one scan pair, Scan $i + 1$ and Scan i (i values range from 1 to $m - 1$);

Table 1. The average normal distance between conjugate points after multiple registrations.

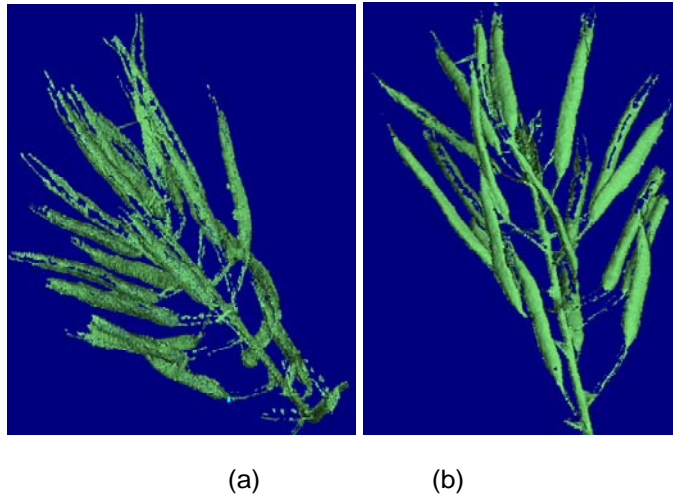| Scan pair	Average normal distances (mm) between matched points before multiple registrations	Average normal distances (mm) between matched points after multiple registrations
30-1	4.78	0.23

(a)   (b)

Figure 7. The results between Scan 1 and the last scan (a) before and (b) after multiple registrations.

$R_i(\Phi_i, \Omega_i, K_i)$ is the rotation matrix between one scan pair, Scan $i + 1$ and Scan l, as defined by the rotation angles Φ_m, Ω_m, K_m (i values range from 1 to m - 1); and S_m is a scale factor between one scan pair, Scan $i + 1$ and Scan i (i values range from 1 to $m - 1$).

Equation (4) could be simplified as follows:

$$SF_1 = F_m(SF_m) \tag{5}$$

where SF_1 is the first scan (Scan 1), SF_m is the last scan (Scan m), and F_m is the transformation function between Scan m and 1 in the indirect way.

Considering all the transformation function between the combined scan pairs and the relations between the last and the first scan, the transformation parameters can be resolved simultaneously according to the following equations:

$$\begin{cases} SF_1 = F_1(SF_2) \\ SF_2 = F_2(SF_3) \\ \dots \\ SF_i = F_i(SF_{i+1}) \\ \dots \\ SF_{n-1} = F_i(SF_{i+1}) \\ SF_1 = F_m(SF_m) \end{cases} \tag{6}$$

This procedure, used to resolve the transformation parameters, was called multiple registrations in our research. Meanwhile, the average normal distance among matched points before and after multiple registrations was also computed. The results are listed in Table 1. The registration results are also presented in Figure 7; Figure 7a shows the result without multiple registrations. There were some disclosures in Figure 7a, whereas there was almost no disclosure shown in Figure 7b, indicating that the multiple registrations were quite effective and necessary.

Surface model generation

The 3D point clouds of the rapeseed were acquired using the method introduced above. To determine the 3D shape of the rapeseed, we used just one set of feature points as well as the interrelations among these points. The TIN model is a simple way to build a surface from a set of irregularly spaced points, making it an attractive method due to its simplicity and economy. Using triangles, each piece of the mosaic surface is placed so as to ensure that it fits its neighboring pieces (that is, the surface is continuous). This is important because the surface of each triangle would be defined by the z coordinates of the three corner points, producing the flat appearance shown in Figure 8. In the TIN model, the points were shown in red and the lines connecting the corner points were shown in purple. The whole rapeseed model from different viewpoints is also presented in Figure 9, which shows that the model is complete and seamless.

RESULTS AND DISCUSSION
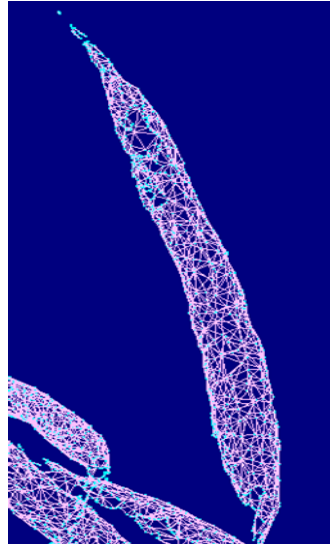
Rapeseed samples at maturity stage were collected and

Figure 8. A rapeseed model at maturity stage by TIN.
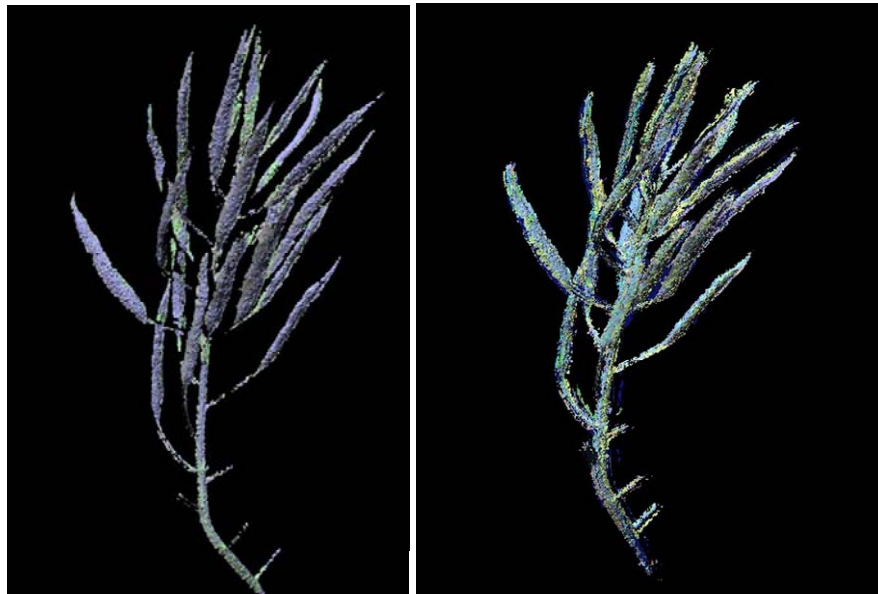

Figure 9. The rapeseed model from different viewpoints.

placed on the turntable controlled by the step motor. Meanwhile, a 3D digitizer was used to acquire data sets of the rapeseed from different viewpoints by rotating the rotatable platform. The proposed methodology was tested to evaluate its performance. In the application, it was applied to reconstruct the surface of one part of a mature rapeseed. A surface model of this part was produced by combining all the scans acquired from different viewpoints. The reconstructed results were also checked to assess their accuracy.

Quantitative assessments of the results

After conducting multiple surface registrations, all the scans were transformed into a common reference frame, which was defined by the first scan, and combined to represent one entire rapeseed model. The average normal distances between the matched points after multiple surface registrations were used as a measure to quantify the quality of registration among all the registered scans. For example, the multiple surface

registrations were performed using 30 scans that have problems of disclosure caused by error propagation of the pair-wise transformation parameters. The experimental results are shown in Table 1, which indicates that the average normal distances between the two scans were less than 0.3 mm after simultaneous registration. However, that value was 4.87 mm before the multiple registrations. The results also demonstrated that all the scans were well combined to a 3D surface model through the multiple surface registration procedure. In addition, the model did not suffer from the error propagation of the pair-wise transformation parameters.

Qualitative assessments of the results

Qualitative assessments of the results of the 3D model were used to confirm the efficiency of the proposed methodology. The assessments were carried out by visually checking the overlapping areas between the first and the last scans in the combined surface model after multiple surface registrations (Figure 7). Specifically, a cross-section of the resulting rapeseed model revealed the quality of registration between scans after the multiple surface registrations. The examination provided information on how well the scans acquired from different viewpoints were registered and combined.

CONCLUSIONS AND FUTURE WORK

The current paper presents a detailed methodology of the automated 3D morphological generation of rapeseed at maturity stage using a 3D digitizer. On the basis of the results of the present study, it can be stated that (1) the 3D digitizer can be used to implement reconstruction of complex organs of plants and 3D shape, and (2) multiple surface registrations are essential for the generation of the 3D shape of rapeseed, leading to better representation and description results compared with other methodologies.

Our future work aims to focus on the following two main aspects: (1) investigating more rapeseed organs and analyzing the mathematical model of these organs to express them through computer graphics, and (2) integrating the generated 3D shape of the rapeseed organs into an L-system to yield a vivid virtual plant that can represent the 3D growth of rapeseed across all growth stages.

Conflict of Interests

The author(s) have not declared any conflict of interests.

REFERENCES

Guan H (2007). Studies on the leaf information of rapeseed based on the computer vision technology. Master thesis, Hunan Agricultural University, Changsha, China.

Ma Y, Guo Y, Li B (2006). Azimuthal distribution of maize plant leaves determined by 3D digitizer. ACTA AGRONOMICA SINCA. 32(6):791-798.

Masaaki O, Yosuke Y (2005). Measurement of spatial leaf distribution by using 3D digitizer and evaluation of light receiving efficiency of tomato plant. FRUTIC 05, Information and Technology for Sustainable Fruit and Vegetable Production, pp. 363-370.

Dornbushch T, Wernecke P, Diepenbrock W (2007). A method to extract morphological traits of plant organs from 3D point clouds as a database for an architectural plant model. Ecol. Model. pp. 119-129.

Watanabe T, Hanan JS, Room PM, Hasegawa T, Nakagawa H, Takahashi W (2005). Rice morphogenesis and plant architecture: measurement, specification and the reconstruction of structural development by 3D architectural modeling. Ann. Bot. 95(7):1131-1143. http://dx.doi.org/10.1093/aob/mci136; PMid:15820987

Yuan D, Liu A, Yuan B (2009). Nutrition information extraction of rape canopy based on computer vision technology. Trans. CSAE 25(12):174-179.

Zhang X, Pan Z, Chen L, Yin J, Li J (2006). Seed color detection by computer technology in rapeseed. Chin. J. Oil Crop Sci. 28(1):11-15.